Tech Science Press

A Fast and Accurate Vascular Tissue Simulation Model Based on Point Primitive Method

Xiaorui Zhang[1,2,*], Hailun Wu[1], Wei Sun[1], Aiguo Song[3] and Sunil Kumar Jha[4]

[1]Jiangsu Engineering Center of Network Monitoring, Engineering Research Center of Digital Forensics, Ministry of Education, School of Computer and Software, Nanjing University of Information Science & Technology, Nanjing, 210044, China
[2]Jiangsu Collaborative Innovation Center on Atmospheric Environment and Equipment Technology, Nanjing University of Information Science & Technology, Nanjing, 210044, China
[3]State Key Laboratory of Bioelectronics, Jiangsu Key Lab of Remote Measurement and Control, School of Instrument Science and Engineering, Southeast University, Nanjing, 210096, China
[4]Faculty of Information Technology, University of Information Technology and Management in Rzeszow, Rzeszow, 35-225, Poland
*Corresponding Author: Xiaorui Zhang. Email: zxr365@126.com
Received: 30 August 2020; Accepted: 14 February 2021

Abstract: Virtual surgery simulation is indispensable for virtual vascular interventional training system, which provides the doctor with visual scene between catheter and vascular. Soft tissue deformation, as the most significant part, determines the success or failure of the virtual surgery simulation. However, most soft tissue deformation model cannot simultaneously meet the requirement of high deformation accuracy and real-time interaction. To solve the challenge mentioned above, this paper proposes a fast and accurate vascular tissue simulation model based on point primitive method. Firstly, the proposed model simulates a deformation of the internal structure of the vascular tissue by adopting a point primitive method. Besides, the stretching constraint and elastic potential energy constraint are introduced to control and correct node motion. Furthermore, a mapping function from the interior to the surface of the vascular tissue is constructed based on moving least squares algorithm to render the visual effect of deformation. Finally, a training system based on the proposed model is set up on the PHANTOM OMNI force-tactile feedback device to realize the deformation simulation of the virtual vascular tissue. Experimental results shows that the proposed model can enhance real-time performance of the training system under the premise of ensuring deformation accuracy, as well as simulate the elasticity of soft tissue.

Keywords: Soft tissue deformation; virtual vascular interventional training system; point primitive method; elastic potential energy constraint; mapping function

1 Introduction

Due to the development of the social economy and the improvement of people's living standards, vascular diseases occur frequently in the middle-aged and elderly population in China. So far, minimally invasive vascular interventional surgery is the most direct and effective treatment method for vascular

diseases [1]. Minimally invasive vascular interventional surgery has been widely used as it has the advantages, such as little traumas and pain, as well as short postoperative recovery time compared with traditional surgery [2]. But the existing vascular interventional surgeries do not meet the requirement of patients for minimally invasive surgeries, resulting in a low rescue-rate and high mortality in vascular diseases. With the advance of virtual surgery, the virtual vascular interventional training system provides a promising application prospect for vascular interventional surgery. It provides surgeons with a good training platform and assistance in visual and tactile sense, and enables repeated surgical trials, thus improving surgeons' technical level. Meanwhile, the usage of virtual vascular interventional training systems can save training costs on real corpses and help in avoiding some ethical issues [3,4].

Although the virtual vascular interventional training system has many advantages for the treatment of vascular diseases, there are still some challenges that need to be solved or balanced when it is set up. At present, the mass-spring model [5–8], finite element model [9–13], mesh-less model [14–18], and tensor-mass method [19] are major physical modeling methods. Many researchers have paid more attention to the vascular model based on these four methods and obtained certain achievements. Wang et al. [20] have used vascular mechanical properties to determine spring coefficients in the mass-spring model, thereby improving the deformation accuracy but reducing the real-time performance. Wu et al. [21] have considered relations between the forces and spring deformation such as elongation and bending based on a traditional mass-spring model, and simulated vascular deformation by optimizing the model parameters with the help of Gaussian processes. This method improves the model stable but degrades the deformation accuracy. Hu et al. [22] have proposed a new mass-spring model based on domain constraint. It achieves a real-time performance but cannot meet the deformation accuracy. Liu et al. [23] have put forward an optimized finite element model, where the Quasi-Newton algorithm is used to accelerate deformation computation, thereby improving the real-time performance of the model. Ye et al. [24] have adopted a spatial adaptive acceleration algorithm in the context of a mesh-less model to accelerate the deformation computation for the vascular model. This algorithm enables a real-time operation but fails in the deformation accuracy. Guo et al. [25] have employed the implicit Euler solver and CG-linear solver to accelerate the deformation computation for the triangular tensor-mass model. This method enhances real-time performance of the model, but the deformation accuracy is not high because it only simulates the surface of the vascular tissue. One year later, they proposed a tetrahedral tensor-mass model to simulate the interior structure of vascular tissue. This model effectively improves the deformation accuracy but fails to improve its real-time performance [26]. As is stated above, accurate vascular deformation effects can be obtained only using high-precision physical modeling methods, but this kind of method will reduce the real-time performance of the training system to some extent. Therefore, how to effectively balance the accuracy and real-time performance during simulating deformation of soft tissues is still a challenge.

To address above challenges, this study proposes a fast and accurate vascular tissue simulation model based on a point primitive method. The proposed model can trade off the deformation accuracy against real-time performance during virtual surgery simulation. During the simulation, a deformation model is constructed based on a point primitive method to capture the motion of nodes modeled inside the vascular tissue. Moreover, stretching constraint and elastic potential energy constraint are employed to simulate the elasticity of vascular tissue by adjusting the node motion. And then a mapping function from interior to the surface of vascular tissue is built to render the deformation with the help of the moving least square algorithm.

The rest part of the paper is organized as follows. Section 2 elaborates on the vascular tissue simulation model based on point primitive method. Then, experimental results and analysis to verify the performance of the proposed vascular tissue simulation model are presented and discussed in Section 3. Finally, the conclusion is presented in Section 4.

2 Method

The framework of our proposed model in the virtual vascular interventional training system is shown in Fig. 1. The framework includes virtual environment establishment, vascular tissue deformation and interaction between doctors and virtual vascular tissue through PHANTOM OMNI. The vascular tissue deformation is be made up of the deformation model constructing, constraints conducting and mapping function building.
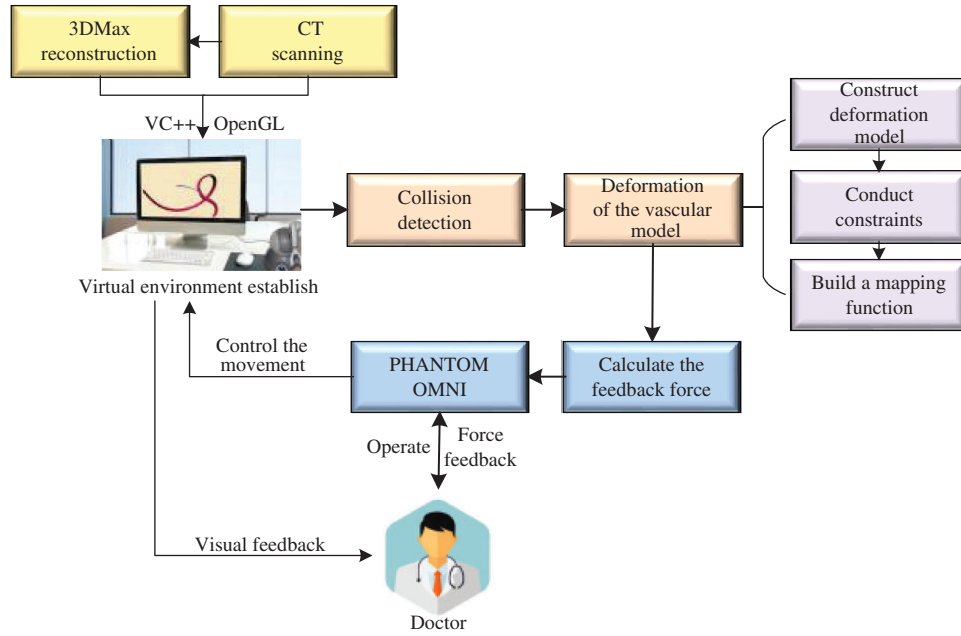

Figure 1: Framework of our proposed model

2.1 Deformation Model

This study uses the point primitive method to construct a deformation model. The main idea of the method is to use a set of discrete nodes to calculate the stress and strain generated by the soft tissue deformation. Then, based on the obtained stress and strain values, displacement of each node is calculated in deformation, thereby capturing vascular tissue deformation.

Assuming that the internal structure of the vascular tissue can be discretized into N nodes, and each node $i(i = 1, 2, \cdots, N)$ has two physical properties including mass m_i and volume v_i. Fig. 2 shows the node support domains inside deformation model. The blue line represents the boundary of vascular tissue surface, the black dots represent the internal nodes, the red area represents the support domain Ω of nodes, and node i is the center node of the support domain, therefore, the rest nodes are neighbors of node i.

The properties of each node are obtained from a kernel function in the support domain. Generally, the smaller the distance between the neighbor nodes and the center node is, the larger effect they have. Therefore, in order to measure the effect of the center node i on its neighbor node j, we used a kernel function to express the relationship as

$$\omega_{ij} = \frac{315}{64\pi h^9} \begin{cases} (h^2 - r^2)^3, & 0 \leq r \leq h \\ 0, & r > h \end{cases} \tag{1}$$
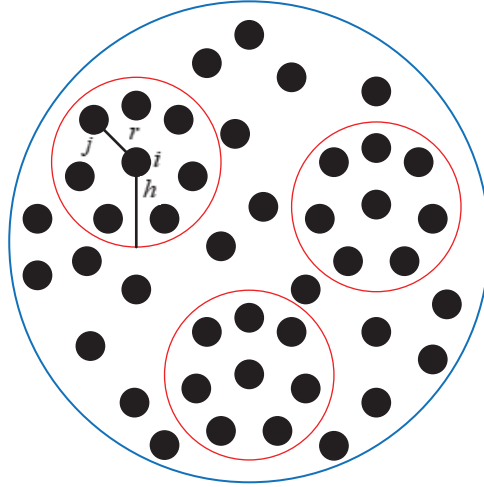
Figure 2: Schematic diagram of node support domains inside vascular tissue

where h is the support radius of the node i and r is the distance between them. Then the spatial derivatives ∇u_i of the displacement vector $u_i = (m, n, p)^T$ are calculated at node i as

$$\nabla u_i = \begin{bmatrix} \nabla m_i \\ \nabla n_i \\ \nabla p_i \end{bmatrix} \qquad (2)$$

where m_i, n_i, and p_i are the x-component, y-component, and z-component of u_i respectively. And ∇m_i can be computed according to Eq. (3)

$$\nabla m_i = A_i^{-1} \sum_j (m_j - m_i)\omega_{ij}(||x_{ij}||)x_{ij} \qquad (3)$$

where ω_{ij} is the mass weight between node i and j which is obtained by Eq. (1), x_{ij} is the difference vector between node i and j, i.e., $x_{ij} = x_i - x_j$, $||x_{ij}||$ is the modulus of the vector x_{ij}, and A_i is the moment matrix. Moreover, A_i can be described as follows

$$A_i = \sum_j \omega_{ij}(||x_{ij}||)x_{ij}x_{ij}^T \qquad (4)$$

Similarly, ∇n_i and ∇p_i are also computed by the mentioned method, to achieve ∇u_i. Furthermore, the strain ε_i and the stress σ_i at node i are obtained based on Eq. (2) as follows

$$\varepsilon_i = J_i^T J_i - I = \nabla u_i + \nabla u_i^T + \nabla u_i \nabla u_i^T \qquad (5)$$

$$\sigma_i = C\varepsilon_i \qquad (6)$$

where J_i is the Jacobi matrix at node i, I is the identity matrix, and C is the elastic matrix, which is determined by Young's modulus and Poisson's ratio.

If the vascular tissue has an elastic deformation under external force, the strain energy will be generated in it. Therefore, we estimate the strain energy U_i stored around node i based on ε_i and σ_i as

$$U_i = \int_\Omega u d\Omega = \int_\Omega \frac{1}{2}(\varepsilon_i \cdot \sigma_i) d\Omega = \frac{1}{2} v_i (\varepsilon_i \cdot \sigma_i) \tag{7}$$

The strain energy is a function of displacement vector u_i and u_j. Taking the derivative with respect to these displacement vectors yields the force acting on node i and j

$$f_j = -\nabla_{u_j} U_i = -v_i \sigma_i \nabla_{u_j} \varepsilon_i \tag{8}$$

$$f_i = -\sum_j f_j \tag{9}$$

It turns out that the force f_i acting on node i is equal to the sum of all f_j acting on its neighbor nodes in magnitude but opposite direction.

Finally, the deformation displacement vector u_i inside the vascular tissue can be solved by Eq. (10) using integration method

$$\frac{d^2 u_i}{dt^2} = \frac{dv_i}{dt} = a_i = \frac{f_{ext} - f_i}{m_i} \tag{10}$$

where v_i and a_i express the velocity and acceleration of node i, respectively, f_{ext} and f_i are the external force and internal force, respectively, and t is the iteration time.

2.2 Construct Constraints

Since the earlier deformation model fails to simulate the biomechanical property of vascular tissue, we added stretching constraint and elastic potential energy constraint in this model using position-based dynamics method. As a result, we can realistically characterize the properties of real vascular tissue.

With the position-based dynamics method, the node positions determined by Eq. (10) is projected to a valid position so that it satisfies the defined constraints, that is, move the node and find a correction factor to modify the deformation position of the node. And the correction factor must meet the following Eq. (11)

$$C(x + \Delta x) \approx C(x) + \nabla_x C(x) \cdot \Delta x = 0 \tag{11}$$

where C is the constraint function. The correction factor of a single node obtained from Eq. (11) is as follows

$$\Delta x_i = -\frac{w_i C(x)}{\sum_j w_j |\nabla_{x_j} C(x)|^2} \nabla_{x_i} C(x) \tag{12}$$

where w_i is the reciprocal of mass m_i.

2.2.1 Stretching Constraint

As shown in Fig. 3, if the distance between nodes is not equal to their original length, the nodes are pulled or pushed by adjusting the stretching constraint to make sure their distance returns to the original length. This solves the problem of mutual penetration between nodes caused by the projection operation. Therefore, the stretching constraint function $C_{distance}(x_1, x_2)$ between any two nodes is defined as

$$C_{distance}(x_1, x_2) = |x_1 - x_2| - d_0 \tag{13}$$

where d_0 is the original length between node x_1 and node x_2. The derivatives of the function $C_{distance}(x_1, x_2)$ are described as
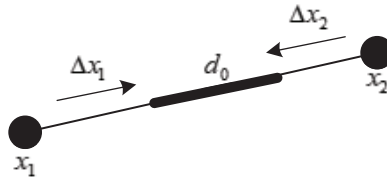
Figure 3: Stretching constraint

$$\nabla_{x_1} C_{distance}(x_1, x_2) = \frac{x_1 - x_2}{|x_1 - x_2|} \tag{14}$$

$$\nabla_{x_2} C_{distance}(x_1, x_2) = -\frac{x_1 - x_2}{|x_1 - x_2|} \tag{15}$$

Hence, the correction factor $\Delta x_i (i = 1, 2)$ of the node under the function of stretching constraint can be derived as follows

$$\Delta x_1 = -\frac{w_1}{w_1 + w_2} (|x_1 - x_2| - d_0) \frac{x_1 - x_2}{|x_1 - x_2|} \tag{16}$$

$$\Delta x_2 = \frac{w_2}{w_1 + w_2} (|x_1 - x_2| - d_0) \frac{x_1 - x_2}{|x_1 - x_2|} \tag{17}$$

2.2.2 Elastic Potential Energy Constraint

The internal structure of the vascular tissue is divided into a set of virtual tetrahedrons based on discrete nodes. Here, an elastic potential energy constraint is designed to describe the elasticity of objects using the spring potential of each tetrahedron with elastic coefficients. As shown in Fig. 4, if the vascular tissue deforms, the spring potential of each deformed tetrahedron will also change correspondingly. Therefore, four nodes of the tetrahedron need to adjust their positions under the function of elastic potential energy constraint to ensure that the vascular model achieves elastic potential energy conservation during simulating the elasticity. Supposing that any two nodes in the tetrahedron are connected by a virtual spring, the elastic potential energy constraint $C_{energy}(x_1, x_2, x_3, x_4)$ is defined as
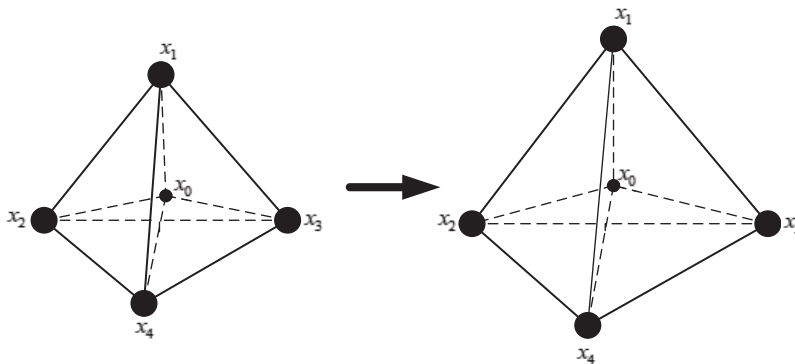

Figure 4: Elastic potential energy constraint

$$C_{energy}(x_1, x_2, x_3, x_4) = \frac{1}{2} \sum_{i=1}^{4} k_{i0}(||x_i - x_0|| - d_{i0})^2 \tag{18}$$

$$x_0 = \sum_{i=1}^{4} m_i x_i / \sum_{i=1}^{4} m_i \tag{19}$$

where x_0 is the barycenter of tetrahedron (x_1, x_2, x_3, x_4), k_{i0} is the elastic coefficient of virtual spring $x_i x_0 (i = 1, 2, 3, 4)$ connecting node x_i and node x_0, and d_{i0} is the original length of $x_i x_0$. The derivatives of the function $C_{energy}(x_1, x_2, x_3, x_4)$ are described as

$$\nabla_{x_1} C_{energy}(x_1, x_2, x_3, x_4) = \frac{x_1 - x_0}{|x_1 - x_0|} \tag{20}$$

$$\nabla_{x_2} C_{energy}(x_1, x_2, x_3, x_4) = \frac{x_2 - x_0}{|x_2 - x_0|} \tag{21}$$

$$\nabla_{x_3} C_{energy}(x_1, x_2, x_3, x_4) = \frac{x_3 - x_0}{|x_3 - x_0|} \tag{22}$$

$$\nabla_{x_4} C_{energy}(x_1, x_2, x_3, x_4) = \frac{x_4 - x_0}{|x_4 - x_0|} \tag{23}$$

Hence, the correction factor Δx_i, i=1, 2, 3, 4 of each node of the tetrahedron under the function of elastic potential energy constraint can be derived as follows

$$\Delta x_i = -\frac{w_i C_{energy}(x_1, x_2, x_3, x_4)}{\sum_j w_j |\nabla_{x_j} C_{energy}(x_1, x_2, x_3, x_4)|^2} \nabla_{x_i} C_{energy}(x_1, x_2, x_3, x_4) \tag{24}$$

The final deformation position of the node that satisfies the stretching constraint and the elastic potential energy constraint is determined by using Eqs. (16), (17), and (24), which guarantees the elasticity of vascular tissue.

2.3 Mapping Function

As illustrated in Section 2.1, the motion of vascular tissue is analyzed with the internal nodes. Thus, we need to establish a mapping function from the interior to the surface of vascular tissue to visualize the deformation process and render the deformation effect based on moving least square algorithm. A set of discrete particles is used to describe the surface structure of vascular tissue, and each surface particle can be represented by the internal nodes in its support domain. The support domain of surface particle X is shown in Fig. 5, in which the blue dots represent the surface particles, the black dots represent the internal nodes, and the circular area represents the support domain S of the surface particle X. Therefore, the mapping function $u(X)$ is defined as

$$u(X) \approx u^h(X) = \Phi(X) U_S \tag{25}$$

$$U_S = [u_1, u_2, \cdots, u_n]^T \tag{26}$$

where $u(X)$ is the field function, which represents the displacement of particle X, $u^h(X)$ is the approximation function of $u(X)$, $\Phi(X)$ is the shape function of particle X, n is the number of internal nodes in the support domain, and U_s is an n-dimensional vector containing the value of the deformation displacement at each node in the support domain.
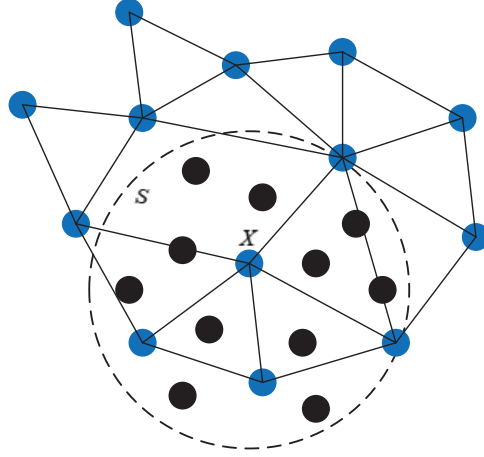
Figure 5: The support domain of surface particle X

The approximation function of the field function $u^h(X)$ is constructed based on moving least square algorithm and $u^h(X)$ is used to express the displacement of particle X. $u^h(X)$ is defined as follows

$$u^h(X) = \sum_{j=1}^{m} p_j(X)a_j(X) = p^T(X)a(X) \tag{27}$$

$$p^T(X) = [p_1(X), p_2(X), \cdots, p_m(X)] \tag{28}$$

$$a(X) = [a_1(X), a_2(X), \cdots, a_m(X)]^T \tag{29}$$

where $p(X)$ is the polynomial basis function and $p^T(X) = [1, x, y, z]$, m is the number of basis function, and $a(X)$ is the coefficient vector, where $a(X)$ can be derived by minimizing the weighted L_2 norm as

$$Q = \sum_{i=1}^{n} w(X - X_i) \left[\sum_{j=1}^{m} p_j(X_i)a_j(X) - u_i \right]^2 \tag{30}$$

where $w(X - X_i)$ is the weight function, X_i is the node in support domain, and u_i is the deformation displacement of node X_i. Besides, we rewrite Eq. (30) in the matrix form as

$$Q = (Pa - U_s)^T W(X)(Pa - U_s) \tag{31}$$

where P is the matrix of basis function and $W(X)$ is the matrix of weight function. Note that P and $W(X)$ are represented as follows

$$P = \begin{bmatrix} p_1(X_1) & p_2(X_1) & \cdots & p_m(X_1) \\ p_1(X_2) & p_2(X_2) & \cdots & p_m(X_2) \\ \vdots & \vdots & & \vdots \\ p_1(X_n) & p_2(X_n) & \cdots & p_m(X_n) \end{bmatrix} = \begin{bmatrix} p^T(X_1) \\ p^T(X_2) \\ \vdots \\ p^T(X_n) \end{bmatrix} \tag{32}$$

$$W(X) = \begin{bmatrix} w(X-X_1) & 0 & \cdots & 0 \\ 0 & w(X-X_2) & \cdots & 0 \\ \vdots & \vdots & & \vdots \\ 0 & 0 & \cdots & w(X-X_n) \end{bmatrix} \tag{33}$$

Finally, derived Eq. (31) with respect to X to obtain the coefficient $a(X)$ as

$$a(X) = A^{-1}(X)B(X)U_s \tag{34}$$

where

$$A(X) = P^T W(X) P \tag{35}$$

$$B(X) = P^T W(X) \tag{36}$$

It can be seen that the weight function plays an important role in constructing the approximate function. Therefore, the cubic spline function is adopted as the weight function, which is defined as

$$W(\mathrm{X}) = \begin{cases} \dfrac{2}{3} - 4s_i{}^2 + 4s_i{}^3, & s_i \le \dfrac{1}{2} \\ \dfrac{4}{3} - 4s_i + 4s_i{}^2 - \dfrac{4}{3}s_i{}^3, & \dfrac{1}{2} < s_i \le 1 \\ 0, & s_i > 1 \end{cases} \tag{37}$$

where $s_i = \dfrac{||X - X_i||}{r_i}$ and r_i is the radius of support domain of particle X_i.

Therefore, the displacement of surface particle X, is obtained, i.e., the field function $u(X)$. The field function based on moving least square algorithm can be expressed as follows

$$u^h(X) = \Phi(X)U_S = \sum_{i=1}^{n} \varphi_i(X)u_i \tag{38}$$

where the shape function is described as

$$\Phi(X) = [\phi_1(X), \phi_2(X), \cdots, \phi_n(X)] = p^T(X)A^{-1}(X)B(X) \tag{39}$$

3 Experiment

3.1 Experiment Environment

All the experiments are based on a desktop with NVIDIA GeForce RTX 2080Ti, Intel(R) Core(TM) i9-9900K CPU (3.60 GHz, 8 cores) and 32G RAM, and run on the Windows 10 operating platform. We adopt VC++ 2019, 3Dmax 2019, and OpenGL 4.6 to program the proposed algorithm and model, and use PHANTOM OMNI hand controller to perform force-tactile interaction operation, which realizes the deformation simulation of the virtual aortic vessels as shown in Fig. 6.

During the simulation, we firstly used 3Dmax software to reconstruct the 3D geometric model of vascular tissue according to the medical CT image. Besides, we employed OpenGL to visually render the vascular model and virtual surgical scene with illumination and texture mapping. Then the operator used the PHANTOM OMNI to interact with vascular tissue through a virtual surgical instrument, resulting in producing deformation under the action of an external force. Finally, the feedback force generated by the deformation is output to PHANTOM OMNI, making the operator feels the feedback force.

Figure 6: Simulation environment

3.2 Simulation Results

To verify the effectiveness of the proposed model and the stability of the virtual vascular interventional training system, we built a straight, bent, and twice bent deformation simulation process for a hand dorsal vein, aortic vessels, and retinal artery vessels, respectively, as shown in Figs. 7, 8, and 9. It can be seen that the deformation process is continuous and the fluent, the deformation effect is realistic when the operator applies the stress to vascular tissues using a virtual catheter.
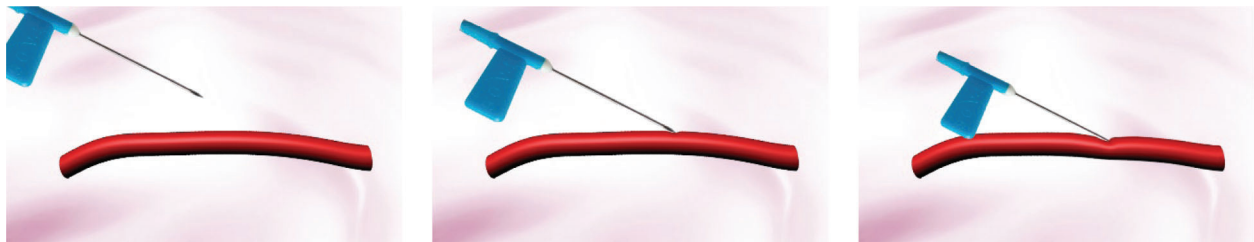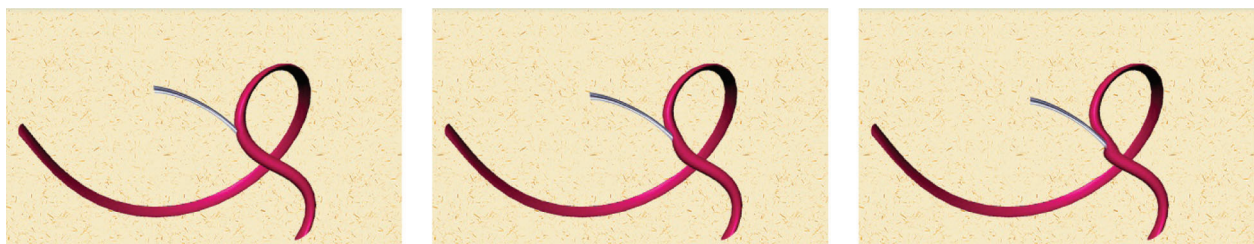

Figure 7: The deformation of hand dorsal vein

Figure 8: The deformation of bent aortic vessels

3.3 Experimental Analysis

3.3.1 Accuracy of Model

This study added the same stress force to real and virtual hand dorsal vein, computed their displacement, and compared the force-displacement curves to verify the accuracy of the proposed model. The mass-spring model [8], the finite element model [23], the tensor-mass method [26], the filling model [27], the position-based dynamics method [16], and the proposed model in this paper are used to conduct the deformation

simulation of virtual hand dorsal vein. Fig. 10 shows the force-displacement curves of real hand dorsal vein and virtual hand dorsal vein based on six different models. From seen Fig. 10, it is obvious that the virtual hand dorsal vein based on the proposed model has a similar force-displacement curve with the real hand dorsal vein, which matches the real curve better than based on other five models.
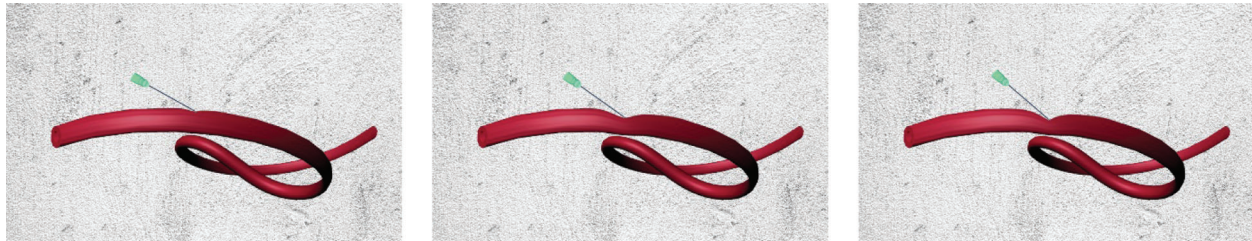

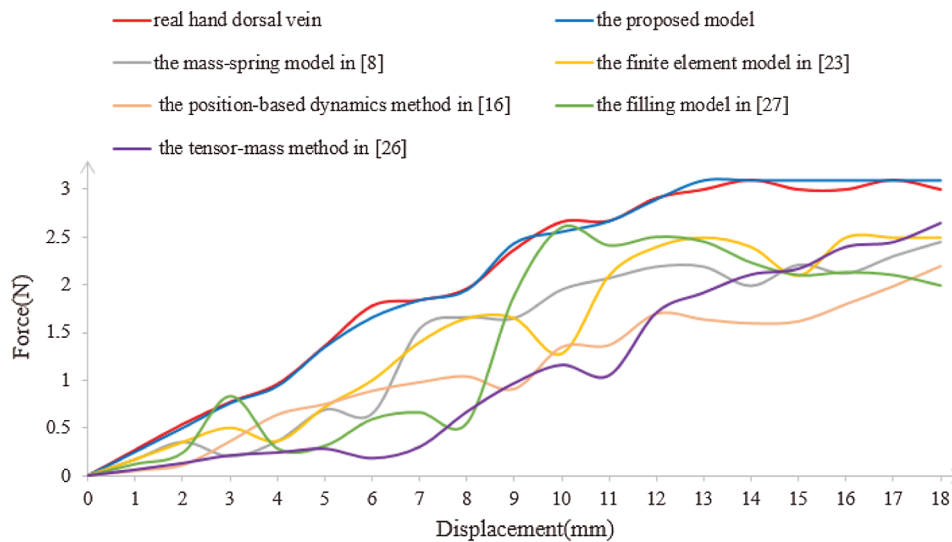**Figure 9:** The deformation of retinal artery vessels under bent twice state

Figure 10: The force-displacement curves of real and virtual hand dorsal veins

3.3.2 Real-time Performance of Model

Real-time performance is a key factor in virtual surgery, because it directly affects the authenticity of a virtual vascular interventional training system. Frames per second (FPS) is an important indicator to measure real-time performance. Commonly, 30 frames can meet the demand for virtual surgery training. Also, the larger the FPS is, the higher the visual refresh rate is, and the better the real-time performance is [28]. Therefore, we used the mass-spring model [8], the finite element model [23], the tensor-mass method [26], the filling model [27], the position-based dynamics method [16], and the proposed model to simulate the deformation based on a different number of vascular nodes. Then, we compared the frames and the deformation time to verify the real-time performance. The deformation time and the frames of different cases are shown in Figs. 11 and 12, from which the proposed model has the least deformation time and the largest frames than the other five models based on same vascular node size. Therefore, the conclusion can be drawn that the real-time performance of the proposed model outperforms the other five models.
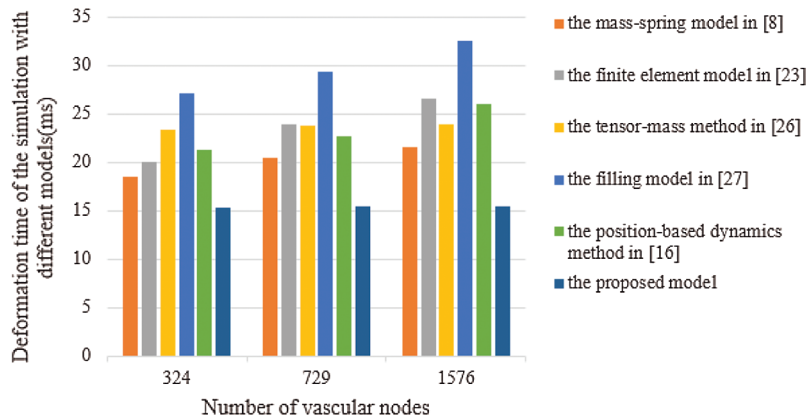
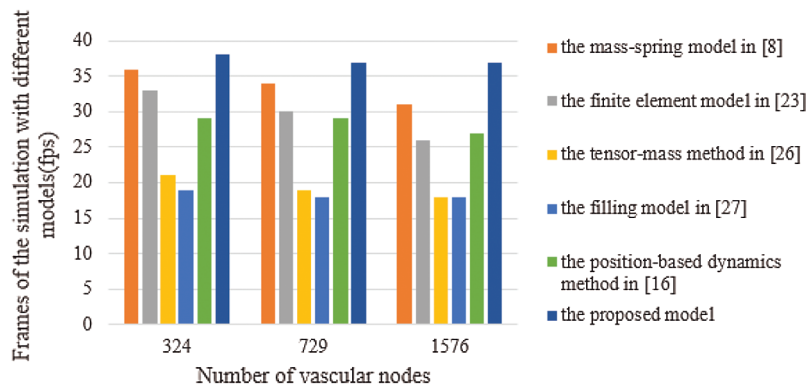**Figure 11:** Deformation time of the simulation with six different models

Figure 12: Frames of the simulation with six different models

3.3.3 Comprehensive Evaluation of Model

The visual characteristic, operational characteristic, and tactile characteristic of the virtual vascular interventional training system directly influence its force-tactile perception performance and friendliness of human-computer interaction. Therefore, the analytic hierarchy process [29] is utilized to verify the force-tactile perception performance of the proposed model by comparing the performance of six different models on the basis of earlier three characteristics. The six models includes the mass-spring model [8], the finite element model [23], the tensor-mass method [26], the filling model [27], the position-based dynamics method [16], and the proposed model.

Analytic hierarchy process, which evaluates the force-tactile perception performance of the simulation system based on the proposed model, is mainly divided into the following three steps:

(1) Establish the hierarchical structure of the evaluation system

The force-tactile perception performance of the simulation system is taken as the evaluated object, and its characteristics are hierarchized to build a hierarchical structure, including the target layer, criterion layer, indicator layer, and scheme layer, which is constructed as shown in Fig. 13. The target layer T indicates the superiority of force-tactile perception performance. The criterion layer C is the first-level evaluation indicator, including visual characteristic C_1, operational characteristic C_2, and tactile characteristic C_3. The indicator layer I is the second-level evaluation indicator, including the image fluency I_1, visual refresh rate I_2, update real-time characteristic I_3, texture characteristic I_4, interaction naturalness I_5,

system stability I_6, deformation accuracy I_7, haptic feedback I_8, and feedback authenticity I_9. The scheme layer S is the six models mentioned previously.
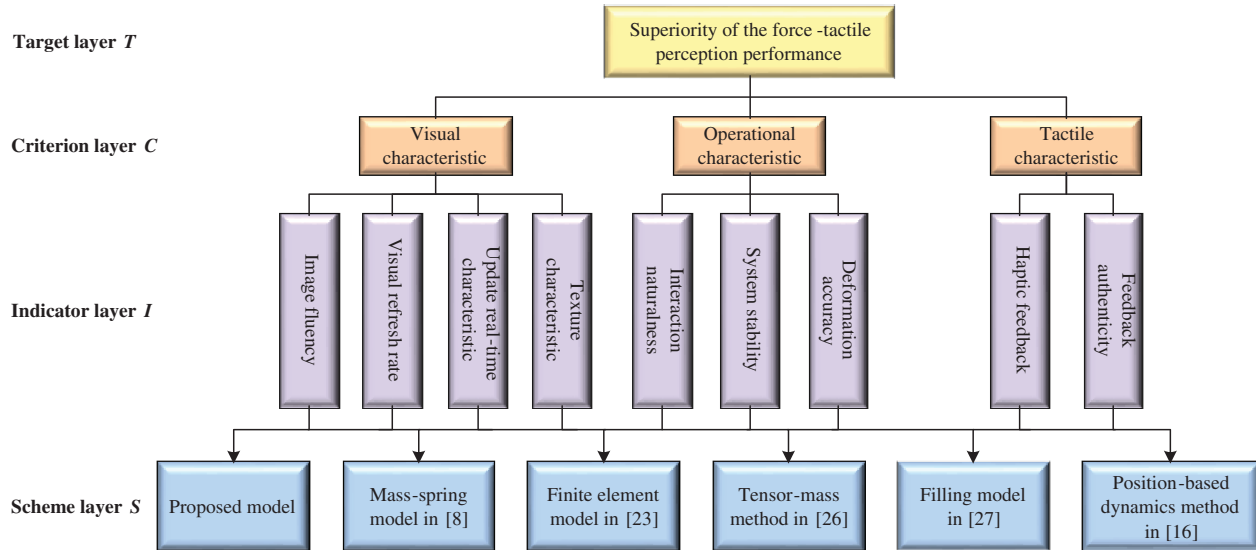

Figure 13: Evaluation system of the force-tactile perception performance

(2) Determine the weight of evaluation indicator

Eighteen doctors have been participating in the study from the first affiliated hospital of Nanjing Medical University, including 8 interns, 3 residents, 4 associate chief physicians, and 3 chief physicians. The doctors score each evaluation indicator based on the 1–9 ratio scale [30] according to the influence of different evaluation indicators on the force-tactile perception performance. The comparison matrix is constructed by combining the opinions of doctors on the score of the evaluation indicator, so that the weight of each evaluation indicator can be calculated and the consistency of the comparison matrix can be checked, as shown in Tab. 1.

Table 1: Weight assignment for force-tactile perception performance evaluation

Criterion layer (C_i)	Weight of criterion layer (W_{C_i})	Indicator layer (I_i)	Weight of indicator layer (W_{I_i})	Consistency check	Comprehensive weight of evaluation indicator (W_i)
Visual characteristic C_1	0.106	I_1	0.567	consistency	0.060
		I_2	0.056		0.006
		I_3	0.104		0.011
		I_4	0.273		0.029
Operational characteristic C_2	0.633	I_5	0.069	consistency	0.044
		I_6	0.155		0.098
		I_7	0.776		0.491
Tactile characteristic C_3	0.261	I_8	0.125	consistency	0.033
		I_9	0.875		0.228

(3) Comprehensive evaluation result

Firstly, doctors are invited to interact with the virtual vascular tissue simulation system based on the six different models through PHANTOM OMNI. Secondly, please they observe the visual characteristics, operational characteristics, and tactile characteristics carefully and define the evaluation standard of the force-tactile perception performance according to the interaction results, shown in Tab. 2. Thirdly, they grade each evaluation indicator, and finally, the comprehensive score of the force-tactile perception performance of the simulation system is obtained by multiplying each evaluation indicator score and its corresponding weight, as calculated in Eq. (40)

$$G = \sum_{i=1}^{k} W_i \cdot \beta_{I_i}, k = 1, 2, \ldots, 9 \tag{40}$$

where G is the comprehensive score, k is the number of the evaluation indicator in the indicator layer, W_i is the comprehensive weight of evaluation indicator I_i, and β_{I_i} is the score of evaluation indicator I_i.

Table 2: Evaluation standard of the force-tactile perception performance

Evaluation indicator		Evaluation standard				
		≤60	60~70	70~80	80~90	90~100
C_1	I_1	not fluent	general	relative fluent	fluent	extremely fluent
	I_2	≤24Hz	24~45Hz	45~65Hz	65~85Hz	≥85Hz
	I_3	slow	relative slow	general	fast	extremely fast
	I_4	coarse	general	relative clear	clear	extremely clear
C_2	I_5	not natural	general	relative natural	natural	extremely natural
	I_6	bad	relative bad	general	good	excellent
	I_7	low	relative low	general	high	extremely high
C_3	I_8	≤300Hz	300~320Hz	320~340Hz	340~360Hz	≥360Hz
	I_9	bad	relative bad	general	good	excellent

The comprehensive evaluation results of the force-tactile perception performance of the simulation system is summarized in Tab. 3.

Table 3: Comparison of the comprehensive evaluation results

Model	Proposed model	Mass-spring model [8]	Finite element model [23]	Tensor-mass method [26]	Filling model [27]	Position-based dynamics method [16]
CS	94.806	81.372	80.634	80.594	79.820	81.971

Tab. 3 indicates that the proposed model achieved the highest comprehensive score. It means the virtual vascular interventional training system based on our model has the best force-tactile perception performance, better visual characteristics, operational characteristics, and tactile characteristics.

4 Conclusion

In this paper, we proposed a fast and accurate vascular tissue simulation model based on point primitive method in a virtual vascular interventional training system. The deformation simulation is built on PHANTOM OMNI force-tactile feedback device with 3Dmax 2019, VC++ 2019, and OpenGL 4.6. This method establishes a deformation model to control the motion of the nodes using the point primitive method inside the vascular tissue. Besides, in this deformation model, the stretching constraint and elastic potential energy constraint are added to characterize the elasticity of soft tissue. In addition, the mapping function from the interior to surface of the vascular tissue is constructed to render the deformation effect. Experimental results show that the proposed model not only provides high deformation accuracy, but also has a fast real-time performance.

To apply the proposed model to a virtual vascular interventional training system, the force feedback needs to provide high fidelity. Follow-up research will focus to more accurate calculation, high-efficiency data processing. Furthermore, this study only simulated the deformation of vascular tissue due to the limitation of CPU computational power, which did not consider further interactions and simulations after deformation, such as constructing the cutting and bleeding simulations. In the future, we will attempt to study the cutting simulation of the vascular tissue by accelerating the deformation computation with the aid of GPU.

Conflicts of Interest: The authors declare that they have no conflicts of interest to report regarding the present study.

References

[1] J. Guo and S. X. Guo, "Design and characteristics evaluation of a novel VR-based robot-assisted catheterization training system with force feedback for vascular interventional surgery," *Microsystem Technologies*, vol. 23, no. 8, pp. 3107–3116, 2017.

[2] S. Lee, S. Shim, H. Ha, H. Lee and J. Hong, "Simultaneous optimization of patient-image registration and hand-eye calibration for accurate augmented reality in surgery," *IEEE Transactions on Biomedical Engineering*, vol. 67, no. 9, pp. 2669–2682, 2020.

[3] B. Martin-Perez, H. Bennis and A. M. Lacy, "Virtual reality simulation for surgery: From video games to transanal total mesorectal excision," *Techniques in Coloproctology*, vol. 22, no. 1, pp. 5–6, 2018.

[4] D. Luo, Y. Zhang and R. Y. Zhao, "Study on deformation technology of virtual surgery simulator based on liver puncture," in *Proc. ICRAE*, Guangzhou, China, pp. 176–179, 2018.

[5] X. R. Zhang, X. F. Yu, W. Sun and A. G. Song, "An optimized model for the local compression deformation of soft tissue," *KSII Transactions on Internet and Information Systems*, vol. 14, no. 2, pp. 671–686, 2020.

[6] X. R. Zhang, J. L. Duan, W. Sun and S. K. Jha, "A tumour perception system based on a multi-layer mass-spring model," *International Journal of Sensor Networks*, vol. 31, no. 1, pp. 24–32, 2019.

[7] X. R. Zhang, J. L. Duan, J. Liu and N. I. Badler, "An integrated suture simulation system with deformation constraint under a suture control strategy," *Computers, Materials & Continua*, vol. 60, no. 3, pp. 1055–1071, 2019.

[8]   C. Q. Li, J. J. Ding, Z. C. Hong, Y. C. Pan and P. X. Liu, "A surface mass-spring model with new flexion springs and collision detection Algorithms based on volume structure for real-time soft-tissue deformation interaction," *IEEE Access*, vol. 6, pp. 75572–75597, 2018.

[9]   W. H. Kim, E. S. Song, K. W. Ju, J. H. Lee, M. Y. Kim *et al.,* "Finite element analysis of novel separable fixture for easy retrievement in case with peri-implantitis," *Materials*, vol. 12, no. 2, pp. 235, 2019.

[10] R. Q. Fuentes-Aguilar, J. C. Bello-Robles and J. Ruiz-León, "Modeling of soft object deformation using finite element differential neural networks," *IFAC PapersOnLine*, vol. 51, no. 13, pp. 474–478, 2018.

[11] W. G. Hou, P. X. Liu and M. H. Zheng, "A new model of soft tissue with constraints for interactive surgical simulation," *Computer Methods and Programs in Biomedicine*, vol. 175, no. Suppl. 1, pp. 35–43, 2019.

[12] J. N. Zhang and S. Chauhan, "Fast computation of soft tissue thermal response under deformation based on fast explicit dynamics finite element algorithm for surgical simulation," *Computer Methods and Programs in Biomedicine*, vol. 187, no. 6–8, pp. 105244, 2020.

[13] P. G. M. Knoops, A. Borghi, R. W. F. Breakey, J. Ong, N. U. O. Jeelani *et al.,* "Three-dimensional soft tissue prediction in orthognathic surgery: A clinical comparison of Dolphin, ProPlan CMF, and probabilistic finite element modelling," *International Journal of Oral and Maxillofacial Surgery*, vol. 48, no. 4, pp. 511–518, 2019.

[14] S. A. Heredia-Perez, K. Harada, M. A. Padilla-Castaneda, M. Marques-Marinho and J. A. Marquez-Flores, "Virtual reality simulation of robotic transsphenoidal brain tumor resection: Evaluating dynamic motion scaling in a master-slave system," *International Journal of Medical Robotics and Computer Assisted Surgery*, vol. 15, no. 1, pp. e1953, 2019.

[15] Y. N. Zou, P. X. Liu, Q. Q. Cheng, P. H. Lai and C. Q. Li, "A new deformation model of biological tissue for surgery simulation," *IEEE Transactions on Cybernetics*, vol. 47, no. 11, pp. 3494–3503, 2017.

[16] L. Xu, Y. H. Lu and Q. Liu, "Integrating viscoelastic mass spring dampers into position-based dynamics to simulate soft tissue deformation in real time," *Royal Society Open Science*, vol. 5, no. 2, pp. 171587, 2018.

[17] J. J. Pan, S. Z. Yan, H. Qin and A. Hao, "Real-time dissection of organs via hybrid coupling of geometric metaballs and physics-centric mesh-free method," *Visual Computer*, vol. 34, no. 1, pp. 105–116, 2018.

[18] Y. J. Peng, Q. L. Li, Y. Y. Yan and Q. Wang, "Real-time deformation and cutting simulation of cornea using point based method," *Multimedia Tools and Applications*, vol. 78, no. 2, pp. 2251–2268, 2019.

[19] B. Gao, L. Shang, X. Cai, Y. Jiang and S. Yang, "Blood flow simulation of virtual simulation system for vascular interventional surgery," in *Proc. ICMA*, Tianjin, China, pp. 2245–2250, 2019.

[20] Y. Wang, S. X. Guo and B. F. Gao, "Vascular elasticity determined mass-spring model for virtual reality simulators," *International Journal of Mechatronics and Automation*, vol. 5, no. 1, pp. 1–10, 2015.

[21] D. M. Wu, C. S. Lv and Y. D. Bao, "An improved vascular model based on mass spring model and parameters optimization by Gaussian Processes," in *Proc. ICMA*, Harbin, China, pp. 2425–2430, 2016.

[22] J. Q. Hu, Y. J. Feng, S. Q. Zhou, L. P. Huang, Q. R. Zeng *et al.,* "An improved mass spring model based on internal point set domain constraint," in *Proc. CCDC*, Chongqing, China, pp. 6826–6831, 2017.

[23] X. H. Liu and J. F. Yao, "Modelling and simulation of vascular tissue based on finite element method," in *Proc. ICISCE*, Zhengzhou, China, pp. 336–340, 2018.

[24] X. F. Ye, J. G. Zhang, P. Li, T. Wang and S. X. Guo, "A fast and stable vascular deformation scheme for interventional surgery training system," *BioMedical Engineering OnLine*, vol. 15, no. 1, pp. 572, 2016.

[25] S. X. Guo, X. J. Cai, B. F. Gao, Q. X. Yang, Y. Zhao *et al.,* "Tensor-mass model based real-time simulation of vessels deformation and force feedback for the interventional surgery training system," in *Proc. ICMA*, Takamatsu, Japan, pp. 433–438, 2017.

[26] S. X. Guo, X. J. Cai and B. F. Gao, "A tensor-mass method-based vascular model and its performance evaluation for interventional surgery virtual reality simulator," *International Journal of Medical Robotics and Computer Assisted Surgery*, vol. 14, no. 6, pp. e1946, 2018.

[27] X. F. Ye, X. K. Mei and S. G. Xiao, "Filling model based soft tissue deformation model," in *Proc. ICMA*, Changchun, China, pp. 1655–1659, 2018.

[28] Y. J. Peng, Y. R. Ma, Y. H. Wang and J. L. Shan, "The application of interactive dynamic virtual surgical simulation visualization method," *Multimedia Tools and Applications*, vol. 76, no. 23, pp. 25197–25214, 2017.

[29] G. Guidi, M. Sliskovic, A. C. Violante and L. Vukic, "Application of the analytic hierarchy process (AHP) to select the best oil spill cleanup method in marine protected areas for calm sea condition," *Global Nest Journal*, vol. 22, no. 7, pp. 354–360, 2020.

[30] S. Lina, "Analysis of factors affecting investment efficiency based on analytic hierarchy process and support vector machine (SVM) model," *Cluster Computing*, vol. 22, no. S2, pp. 4367–4374, 2019.